Iron overload alters iron-regulatory genes and proteins, down-regulates osteoblastic phenotype, and is associated with apoptosis in fetal rat calvaria cultures

By: Jonathan G. Messer, Amy K. Kilbarger, Keith M. Erikson, Deborah E. Kipp,

Messer, J.G., Kilbarger, A.K., Erikson, K.M., Kipp, D.E. (2009) Iron overload alters iron-regulatory genes and proteins, down-regulates osteoblastic phenotype, and is associated with apoptosis in fetal rat calvaria cultures. Bone 45: 972-999.

Abstract:

Iron overload has been implicated in decreased bone mineral density. However, the effect of iron overload on osteoblast lineage cells remains poorly understood. The purpose of this study was to examine osteoblast differentiation, function, and apoptosis in iron-loaded cells from fetal rat calvaria. Cells were incubated with media supplemented with 0–10 μM ferrous sulfate ($FeSO_4$) during differentiation (days 6–20). Intracellular iron status was assessed by measuring iron content in cell layers and changes in transferrin receptor (TrfR) and ferritin gene and protein expression. Osteoblast differentiation and function were evaluated by measuring osteoblast phenotypic gene markers and capacity of cultures to form mineralized bone nodules. Apoptotic hallmarks were evaluated by microscopy. A 2.3-fold increase in media iron concentration resulted in saturable accumulation of iron in the cell layer 20-fold higher than control ($p < 0.05$) by mid-differentiation (day 15, D15). Iron accumulation resulted in rapid and sustained down-regulation of TrfR gene and protein levels (within 24 h) and up-regulation of light and heavy chain ferritin protein levels at late differentiation (day 20, D20). Concurrently, osteoblast phenotype gene markers were suppressed by D15 and a decreased number of mineralized nodules at D20 were observed. Apoptotic events were observed within 24 h of iron loading. These results provide evidence that iron overload alters iron metabolism and suppresses differentiation and function of cells in the osteoblast lineage associated with increased apoptosis.

Keywords: Osteocalcin, Bone nodules, Transferrin receptor Ferritin, Ferrous sulfate

Article:

Introduction

Iron is essential for many biological processes. However, the value of iron in maintaining growth and survival is offset by its potential to catalyze formation of highly reactive free radicals, which can damage cellular components [1]. Since the human body has no effective mechanism for excreting iron, cells must tightly regulate uptake and store iron safely, in order to prevent detrimental effects of free iron. Increasing iron stores to levels beyond the tolerable threshold of cells, as seen in iron overload disorders, leads to decreased organ functioning (e.g. liver failure), contributing to various diseases. Primary iron overload is due to genetic mutations and results in increased intestinal absorption, while secondary iron overload is generally attributed to repeated blood transfusions, or is the consequence of increased dietary iron, iron supplementation, and aging [2–5].

Iron overload has been linked to bone metabolic disorders, such as osteopenia, osteoporosis, and osteomalacia in humans [6,7] and animals [8–10]. The changes in bone density are often associated with stainable iron in osteoid seam, bone marrow stroma, and osteoblasts [2,7,8]. Additionally, osteoblasts express both the iron uptake protein transferrin receptor (TrfR) and the iron storage protein light and heavy chain subunits of heteromeric ferritin, suggesting that these cells have the ability to accumulate iron [11,12]. Despite the clear implication of iron's effects on bone formation, studies designed to establish the extent to which iron alters osteoblast differentiation and function are lacking. Therefore, the purpose of the present study was to examine differentiation and function of iron-loaded osteoblast-like cells isolated from fetal rat calvaria.

Fetal rat calvaria cultures are a well defined model of osteoblastic differentiation, resulting in the formation of nodules which contain osteoblast-like cells that secrete functional extracellular matrix that becomes mineralized. Cells were exposed to 0– 10 μM concentrations of ferrous sulfate ($FeSO_4$) throughout differentiation and samples were taken during acute (up to 48 h) and chronic (up to 2 weeks) exposure to FeSO4. The 5 μM $FeSO_4$ treatment increased iron 2.3-fold in the media, which is similar to the 2-fold increase in serum iron observed in patients with hemochromatosis [13] and iron-loaded animals with altered bone metabolic parameters [8–10]. Alongside the primary aim of describing osteoblast differentiation and function, iron concentration was evaluated and transferrin receptor and ferritin light (FerL) and heavy (FerH) subunits are described. Since expression of these genes and proteins is canonically regulated by intracellular iron [14], any alteration should indicate a change in intracellular iron status. Finally, evaluation of apoptosis was assessed because iron-induced damage has been shown to lead to programmed cell death in vivo and in vitro [15–17].

Materials and methods

Animal care

Female Sprague–Dawley rats were obtained on day 13 of pregnancy (Harlan, SD, Raleigh, NC) and housed at 19–20 °C with a 12 h light–dark cycle. Dams had free access to Harlan Teklad 7002 6% mouse/rat diet and water. At day 21 of pregnancy, dams were euthanized by CO_2 overdose, pups were collected, and calvaria were aseptically removed [18]. These procedures were approved by the University of North Carolina at Greensboro Animal Care and Use Committee.

Calvaria cultures

Cells were enzymatically released from calvaria in five sequential collagenase digestions as previously described [18]. Cells from the last four incubations were plated in separate T-75 flasks and incubated 24 h in α-MEM (Invitrogen) containing 15% heat-inactivated fetal bovine serum (FBS) (Invitrogen) and 10% antibiotics. Antibiotics consisted of 1 mg/mL penicillin (Sigma), 0.5 mg/mL gentamicin (Invitrogen), and 2.5 μg/mL fungizone (Invitrogen). Cells from each flask were trypsinized, pooled, and seeded at 3000 cells/cm^2 in 6 well plates. Cells were incubated up to 21 days at 37 °C with 5% CO2 and fresh media was provided every 2–3 days. Complete media contained α-MEM, 10% FBS, 10% antibiotics, 25 μg/mL ascorbic acid, 10 mM sodium β-glycerolphosphate, and 10^{-8} M dexamethasone and was used throughout the entire culture period (D1–21). Iron (II) sulfate heptahydrate ($FeSO_4$) (Sigma) was added to complete media at final concentrations of 1–10 μM $FeSO_4$. Deionized water was the vehicle control (0 μM).

Iron concentration of individual media components and complete media with or without addition of $FeSO_4$ was confirmed by graphite furnace atomic absorbance spectrometry (GFAAS) described below. The iron concentration of FBS was 31.5 μmol/L ± 9.55 (n = 2) while other media components had negligible iron concentration. Thus, iron concentration in control media was attributed to 10% FBS and confirmed at 3.07 μmol/L ± 1.03 (n = 2). The addition of 1 and 5 μM $FeSO_4$ increased total iron concentration in complete media to 4.07 μmol/L ± 1.50 (n = 2) and 7.20 μmol/L ± 2.61 (n = 2), or about 1.3- and 2.3-fold higher than control, respectively. Values for 10 μM were not determined by GFAAS.

To observe effects of acute iron exposure, media was changed at confluence (D6–8) and cells were incubated 24 h since growth factors may influence expression of TrfR and iron uptake [19]. $FeSO_4$ was spiked directly into wells 24 h after changing media. To observe chronic effects of iron exposure, $FeSO_4$ was delivered in fresh media beginning at confluence and at subsequent media changes throughout the experiment.

Graphite Furnace Atomic Absorption Spectrometry (GFAAS)

Iron concentration in the cell layer was analyzed on D 15 and D20 of cell culture using a protocol adapted from Erikson and Aschner [20]. Briefly, media was removed and cells were washed twice with PBS. Cell layers (cells and extracellular matrix) were detached from plates by scraping in 1 mL of cell dissociation solution (Sigma) or PBS. If dissociation solution was used, pellets were obtained by centrifugation and washed with PBS before proceeding. Samples were digested in Ultra Pure Nitric Acid (Fisher Scientific) at 60 °C for 48 h in a sand bath and then analyzed with a Varian AA240 atomic absorption spectrometer (Varian Inc.). Average

protein concentration of cell layers (n = 2 wells) was determined by bicinchoninic acid (BCA) assay (Pierce). Iron concentration values are expressed as nmol Fe/mg protein. Media and reagent samples were also diluted in Ultra Pure Nitric Acid and analyzed.

RT-PCR

Cells were collected in 1 mL of TRIZOL (Invitrogen) by scraping and RNA was extracted using the procedures specified by the manufacturer. Isolated RNA was dissolved in nuclease-free water and DNase treated with Turbo DNA-free (Ambion) per manufacturer's instructions. RNA purity and concentration were determined spectro-photometrically at 260 and 280 nm using a Beckman Spectro-photometer. One microgram of RNA was primed with Oligo(dT) (Amersham) and reverse transcribed using Omniscript RT kit (Qiagen) by the manufacturer's instructions. One microliter of diluted cDNA was submitted to PCR reaction using Qiagen Taq polymerase PCR kit. Primer sequences, annealing temperatures, and amplimer sizes are listed in Table 1. Primer sequences designed for this study (alkaline phosphatase, ALP; FerH; FerL) spanned at least one exon/exon boundary. Primer sequences for ribosomal protein L32, collagen 1 (COLL 1), bone sialoprotein (BSP), osteocalcin (OCN), and TrfR were previously described [21,22]. Amplimers were resolved on a 1% agarose gel stained with ethidium bromide. The number of cycles was optimized for each gene within the exponential phase of amplification (not shown). Non-specific amplification due to genomic DNA or reagent contamination was not observed in control lanes (not shown).

Table 1
Primer information.

Primer	Sequence	Annealing temperature	Fragment size
Ribosomal L32[21]	F-CAT GGC TGC CCT TCG GCC TC R-CAT TCT CTT CGC TGC GTA GCC	56 °C	403 bp
Transferrin receptor [22]	F-GGC CGG TCA GTT CAT TAT TA R-CTC ATG ACG AAT CTG TTT GTT	55 °C	237 bp
FerH	F-GCC AGA ACT ACC ACC AGG AC R-CAG GGT GTG CTT TGT CAA AGA	59 °C	500 bp
FerL	F-CCT CTC TCT GGG CTT CTT TTT R-AGG TTG GTC AGG TGG TTG C	61 °C	363 bp
Osteocalcin [21]	F-AGG ACC CTC TCT CTG CTC AC R-AAC GGT GGT GCC ATA GAT GC	56 °C	274 bp
Bone sialoprotein [21]	F-CGC CTA CTT TTA TCC TCC TCT G R-CTG ACC CTC GTA GCC TTC ATA G	56 °C	780 bp
Alkaline phosphatase	F-GAC CTT GAA AAA TGC CCT GA R-CGC ATC TCA TTG TCC GAG TA	56 °C	474 bp
Collagen 1a [22]	F-GGA GAG AGT GCC CAA CTC CAG R-CCA CCC CAG GGA TAA AAA CT	59 °C	207 bp

Western blotting

Cells were lysed in 150 μL of RIPA buffer, containing 10 mM sodium fluoride, 20 mM β-glycerolphosphate, 0.1 mM sodium orthovanadate, and protease inhibitor cocktail (Calbiochem). Lysates were sonicated on ice and centrifuged at 16,000 ×g for 20 min. Supernatants were removed and stored at — 80 °C before protein concentrations were determined with BCA assay (Pierce).

Twenty micrograms of proteins per well was resolved on NuPage 4-12% bis-tris gels (Invitrogen). Proteins were transferred onto polyvinylidene difluoride membranes (Immobilon) and blocked in 5% (w/v) milk dissolved in Tris-buffered saline with 0.05% (w/v) Tween-20 (TBS-T) (Sigma). Membranes were then incubated with primary antibodies overnight at 4 °C, washed in TBS-T, and incubated with secondary antibodies for 30 min at room temperature. Primary antibodies were diluted in 5% (w/v) bovine serum albumin (Sigma) in TBS-T and included mouse anti-β-actin (Sigma), mouse anti-transferrin receptor (Zymed), rabbit anti-ferritin light chain (Alpha Diagnostic) and rabbit anti-ferritin heavy chain (Alpha Diagnostic). HRP-conjugated secondary antibodies include donkey anti-mouse (Affinity BioReagents) and goat anti-rabbit (Cell Signaling). Signal was detected with Western Lightning Chemiluminescence Reagent Plus kit (PerkinElmer).

Staining

These methods are described in detail elsewhere [23]. Briefly, cells were washed in PBS, fixed in 10% neutral formalin buffer, and rinsed with deionized water. ALP-positive cells were stained using Naphthol AS MX-PO_4 (Sigma) as substrate and Red Violet LB salt (Sigma) as coupler. Mineralized nodules were stained using the von Kossa method by incubating cells with 2.5% (w/v) silver nitrate (Fisher) solution for 30 min. Culture dishes were then rinsed in tap water and air dried overnight. Dishes of stained cells were scanned on a flatbed scanner at a resolution of 600 dpi.

Bone nodule quantification

The numbers of mineralized and unmineralized nodules were counted under bright field illumination in dishes of stained cells set atop a transparent plastic grid. Unmineralized nodules were defined as multilayered areas containing foci of cuboidal cells that were intensely ALP-positive with little or no von Kossa staining. Mineralized nodules were defined as multilayered areas of intensely ALP-positive cells strongly associated with von Kossa staining, which appears brown/ black.

TUNEL assay

Cells were washed in PBS, fixed in 10% neutral formalin buffer and stored at 2 °C up to one week before completing analysis. Endogenous peroxidases were blocked by incubating cells with 0.3% hydrogen peroxide in methanol for 30 min at room temperature. Apoptotic DNA was labeled with *In Situ* Cell Death Detection Kit, POD (Roche Diagnostics) using the manufacturer's instructions for adherent cells. Fluorescent signal was converted to colorimetric indicator using Metal Enhanced DAB Substrate Kit (Pierce) per manufacturer's instruction. Positive controls included hydrogen peroxide (H_2O_2) spiked directly into wells at 150 μM final concentration [24] or incubation of fixed cells with DNase I at 2200 U/mL and 10 mM $MgCl_2$ for 30 min at room temperature just before performing the assay.

Annexin V, propidium iodide staining

Phosphatidyl serine translocation to the outer cell membrane was labeled with reagents provided in a kit from Roche Applied Science. Staining was performed as indicated in the protocol before analyzing with fluorescence microscopy. Apoptotic cells appeared green and were distinguished from necrosis and secondary necrosis by costaining cells with propidium iodide, which appears red. Hydrogen peroxide (H_2O_2) was used as a positive, treatment control.

Assessment of cell death staining

Cells were evaluated microscopically on an Olympus IX70 microscope and representative fields were photographed at 100×. Images were scored on a 4-point scale based on the intensity of the stain, where, + + + indicates high staining; + + indicates moderate staining; + indicates low staining; and — indicates no detectable stain. Images from 2 independent studies were analyzed.

Statistical analysis

Data are expressed as mean ± SEM. One-way analysis of variance (ANOVA) was performed with Tukey post hoc analysis for multiple comparisons within the time point evaluated. Statistics were performed using SPSS version 15.0.1 for Windows (SPSS Inc., Chicago, IL, USA). A p-value less than 0.05 was considered significant.

Results

Iron concentration

Iron concentration in cell layers is shown in Fig. 1. The 5 μM treatment resulted in significantly higher ($p<0.05$) iron levels in the cell layer by D15 that were approximately 20 times higher than control. Values were similar on D20 and there was no significant difference between 5 and 10 μM $FeSO_4$ ($p > 0.05$). Treatment with 1 μM DFOM did not result in significant iron accumulation compared to control on D15 or on D20 ($p > 0.05$).

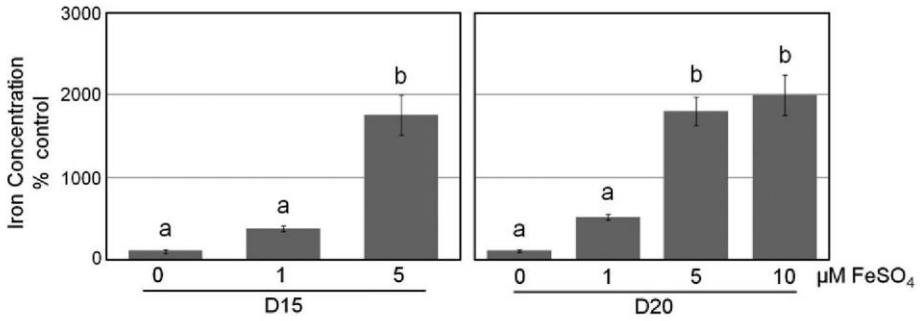

Fig. 1. Iron concentration in the cell layer at D15 and D20. Graphs are percent of control (0 μM). Treatments that are significantly different ($p<0.05$) as determined by Tukey post hoc analysis are assigned different letters. Treatments that are not significantly different ($p>0.05$) are assigned the same letters. Each graph shows results from separate independent studies. Results were similar in 2 (D15) or 3 (D20) independent studies, $n=3$–5 wells per treatment per independent study (except the 10 μM dose, which was only determined in 1 of the independent studies, $n=3$ wells).

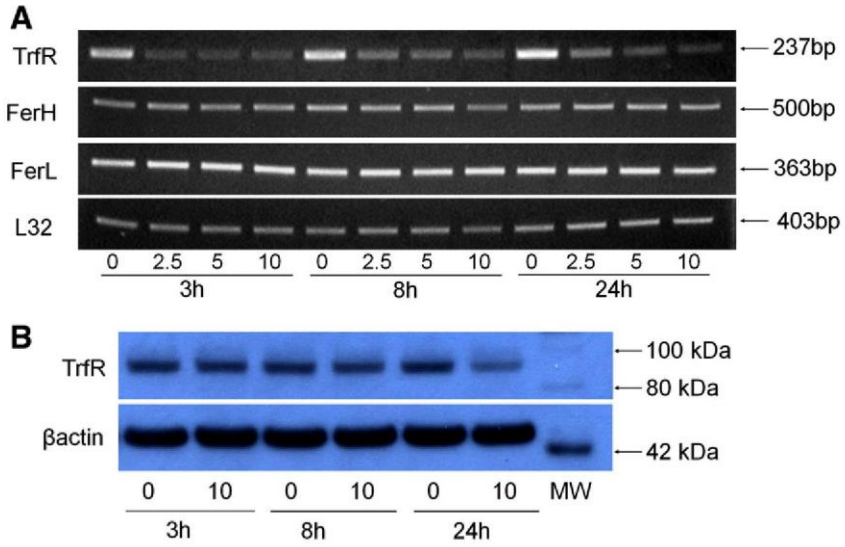

Fig. 2. Iron-regulated gene and protein expression after acute exposure to $FeSO_4$. (A) RT-PCR amplification of TrfR, FerH, FerL, and loading control L32. (B) Western blots of TrfR and loading control β-actin. Representative results from 1 study. Similar results were observed in 2 independent experiments.

Iron-regulated gene and protein expression after acute or chronic $FeSO_4$ treatment

TrfR gene expression was markedly down-regulated between 3 and 48 h after acute exposure to all doses of $FeSO_4$. Data through 24 h is shown in Fig. 2A. FerH and FerL gene expression was not altered at any dose or time point. Congruent with gene expression, TrfR protein was markedly decreased after 24 h of incubation with 10 μM $FeSO_4$ compared to 24 h control (Fig. 2B), and no changes in FerH or FerL protein expression were observed during acute exposure (not shown).

Chronic exposure to 5 μM $FeSO_4$ was associated with down-regulated TrfR gene expression by D15 which was sustained at D20, but no effect was seen on FerL or FerH genes (Fig. 3A). The 5 and 10 μM $FeSO_4$ treatments produced similar effects on gene expression by D20. Down-regulation of TrfR protein matched gene expression after chronic exposure to 5 and 10 μM $FeSO_4$ on D15 (not shown) and D20 (Fig. 3B). In contrast, FerH and FerL proteins were only up-regulated at D20 after chronic exposure to 5 or 10 μM $FeSO_4$ treatments (Fig. 3B).

Function of osteoblast-like cells is suppressed by $FeSO_4$ treatment

Representative cell culture wells and micrographs of typical morphology of nodules at D20 are shown in Figs. 4A and B, respectively. The total number of nodules was similar among treatments ($p > 0.05$). However, the proportion of unmineralized or poorly mineralized nodules increased dose-dependently after chronic exposure to $FeSO_4$, while mineralized nodules exhibited reciprocal trend (Fig. 4C).

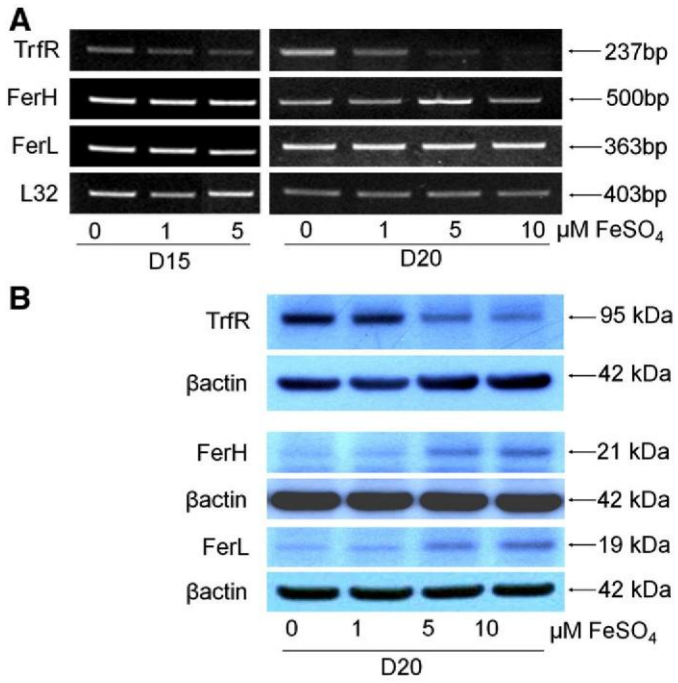

Fig. 3. Iron-regulated gene and protein expression after chronic exposure to $FeSO_4$. (A) RT-PCR amplification of TrfR, FerH, FerL, and loading control L32 on D15 and D20. (B) Western blots of TrfR, FerH, FerL and loading control β-actin on D20. Representative results from 1 study. Similar results were observed in 2 to 3 independent experiments.

Osteoblast phenotype gene markers are down-regulated by $FeSO_4$ treatment

Genes characteristic of the osteoblast phenotype are expressed in a well-described, time-dependent pattern in fetal rat calvaria cell cultures [25]. Generally, COLL1 up-regulation is followed by ALP and BSP while the most specific osteoblast phenotype marker, OCN, is highly expressed at the end of culture. The 5 μM $FeSO_4$ treatment markedly suppressed osteoblast phenotype genes, particularly BSP and OCN, by D15 in culture (Fig. 5). Similar results are seen on D20, however, 10 μM $FeSO_4$ had the most pronounced suppressive effect in comparison to control.

Acute iron exposure is associated with apoptotic events

Condensed, TUNEL-positive nuclei were generally observed in cells treated with iron and resembled the labeled nuclei detected after treatment with 150 μM hydrogen peroxide (Fig. 6, Table 2). Iron-treated cells achieved moderate staining intensity compared to low staining intensity in 0 μM, while all nuclei were labeled in DNase I-treated control cells. Apoptosis in iron-treated cells was confirmed by observation of phosphatidyl serine translocation labeled by Annexin V antibody (Fig. 7, Table 3). Treatments resulted in staining intensity that was similar to that of TUNEL assay. A moderate degree of Annexin V/propidium iodide costaining was observed in nodules in all treatments, indicating necrotic cell death or secondary necrosis, which occurs in later stages of apoptosis.

Discussion

This is the first report describing iron accumulation in osteoblasts *in vitro*. Increased intracellular iron concentration is associated with suppressed osteoblast differentiation and function, which is consistent with decreased bone mineral density *in vivo*. Acute iron exposure is also associated with cell death characteristic of apoptosis.

Iron concentrations in osteoblast cell layers remained low after chronically elevating iron 1.3-fold (1 μM $FeSO_4$). The 2.3-fold higher treatment (5 μM $FeSO_4$) resulted in saturated iron levels in the cell layer by D15. Similarly, primary hepatocytes, astrocytes, and HepG2 cells exposed to excess iron effectively prevent intracellular iron accumulation at low doses, while higher doses result in time-dependent plateau of iron accumulation [26–28].

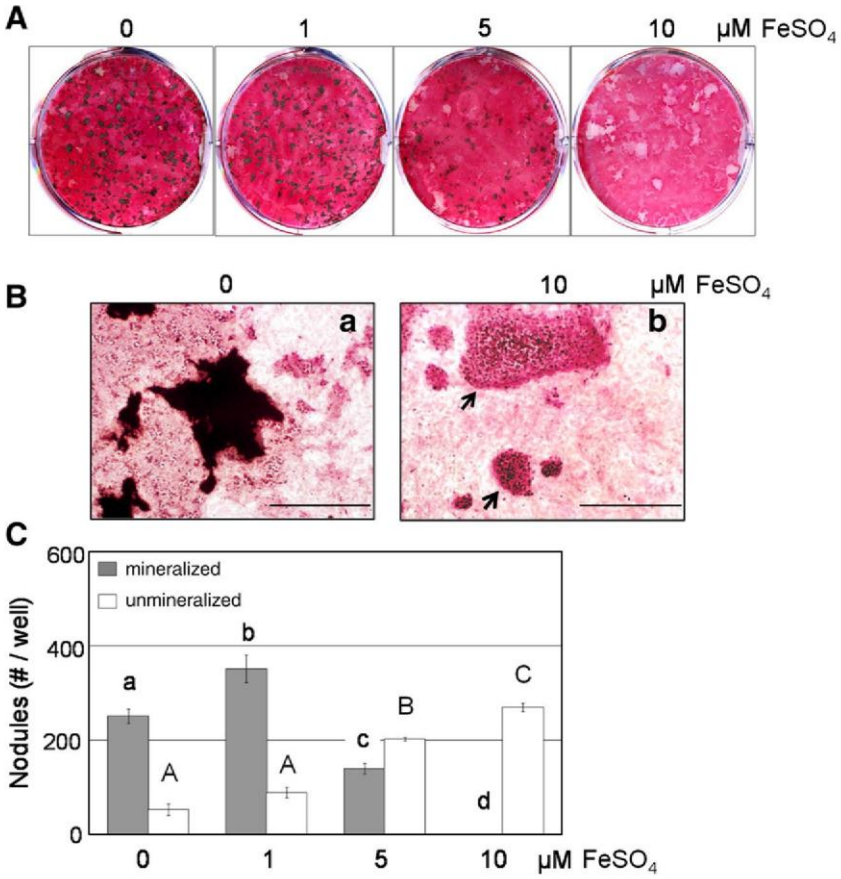

Fig. 4. Bone nodules on D20 after chronic exposure to $FeSO_4$. (A) Stained wells of alkaline phosphatase positive-colonies (pink) and mineralized nodules (black/brown). (B) 100× micrographs of (a) well-mineralized, opaque nodules in control wells and (b) unmineralized nodules (arrows) from cells treated with 10 μM $FeSO_4$. Scale bar: 500 μm. (C) Average number of nodules per well. Mineralized and unmineralized nodules were analyzed separately. ANOVA: $p<0.05$ for each group. Differences were determined by Tukey post hoc analysis. Treatments resulting in significantly different ($p<0.05$) outcomes are indicated by different letters. Treatments not significantly different ($p>0.05$) are assigned the same letters. Capital letters correspond to unmineralized group, lower case letters correspond to mineralized group. Representative results from 1 study. Similar results were observed in 2 to 3 independent experiments.

Coinciding modulation of gene and protein levels of TrfR and ferritin is consistent with intracellular iron accumulation, although iron concentration was determined from the entire cell layer, and therefore some iron may have been located within the extracellular matrix. The occurrence of extracellular iron accumulation in bone is supported by literature in which iron staining in noncellular osteoid has been observed.

Unlike other cell types, the regulation of iron metabolism in osteoblasts has not been studied extensively. In the present study, it appears that the plateau in intracellular iron concentration is a result of the rapid and sustained down-regulation of TrfR protein. However, post-translational glycosylation and phosphorylation of TrfR have been reported, suggesting that modification of TrfR activity as well as participation by other iron-handling proteins could fine-tune iron uptake in osteoblast-like cells [4,29,30]. Classical iron-mediated up-regulation of ferritin involves increased translation, which is consistent in the present study on D20, in which proteins are up-regulated in the absence of detectable up-regulation of mRNA levels. However, it was surprising that the up-regulation did not coincide with saturation of iron levels at D 15. The reason for this remains unclear but alludes to the possibility that FerH and FerL regulation in osteoblasts relies on signals other than intracellular iron. It appears that, beyond direct regulation by iron, transcriptional and post-transcriptional regulation of ferritin subunits depends on both stimulus and cell type [31]. Furthermore, ascorbic acid is a known regulator of ferritin metabolism but is required in calvaria-derived osteoblastic cell cultures for appropriate collagen formation and matrix maturation [32], thus potentially confounding *in vitro* results.

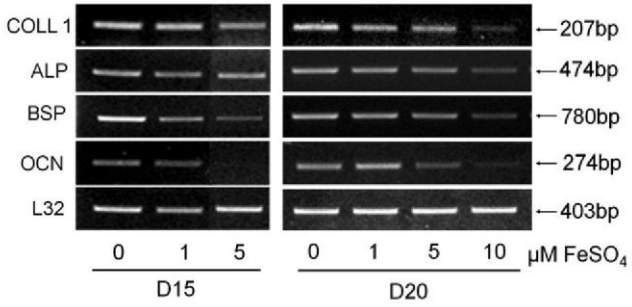

Fig. 5. Osteoblast phenotype gene expression after chronic exposure to $FeSO_4$. RT-PCR amplification of COLL 1, ALP, BSP, OCN, and loading control, ribosomal protein L32 on D15 and D20. Representative results from 1 study. Similar results were observed in 2 to 3 independent experiments.

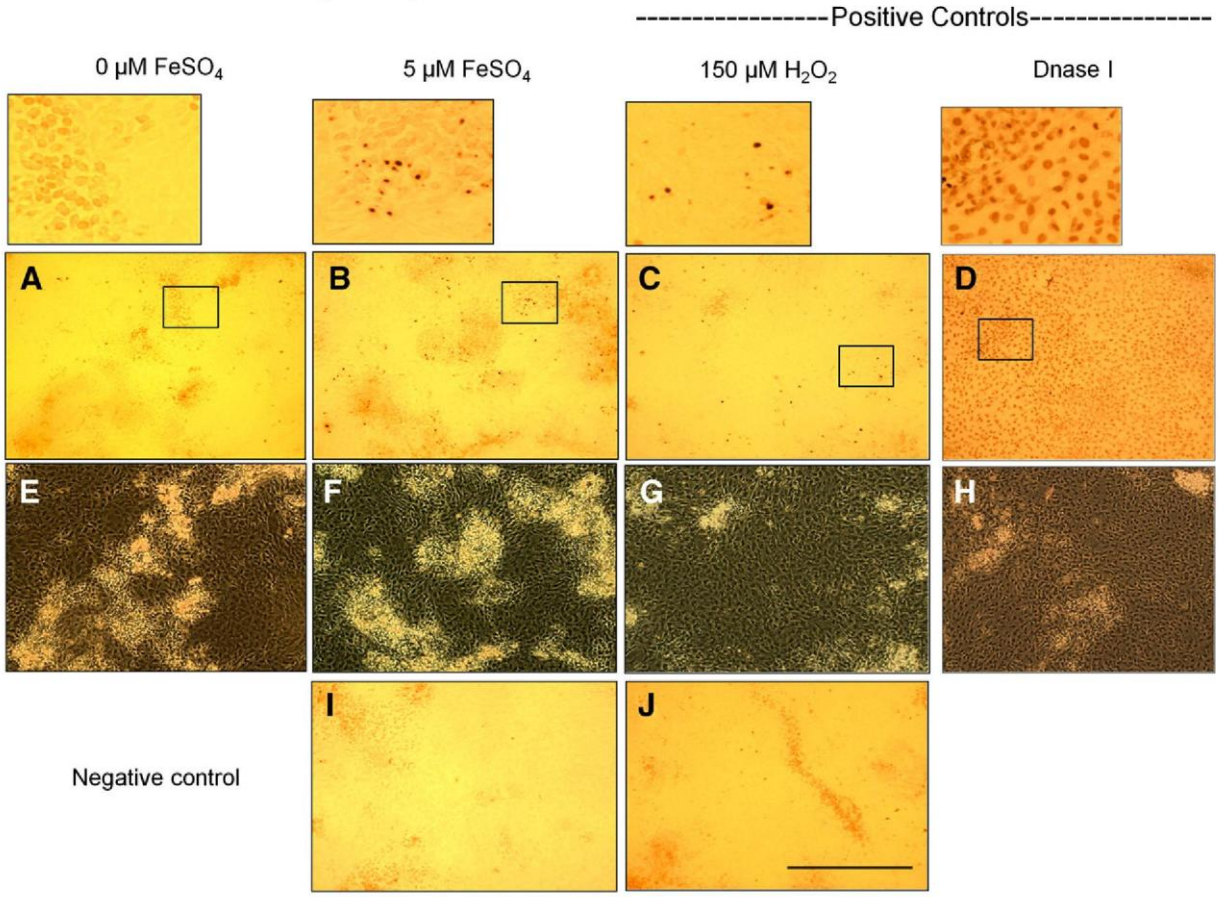

Fig. 6. TUNEL-labeled nuclei after acute $FeSO_4$ treatment. (A–C) Bright field images of cells treated 24 h with 0 or 5 μM $FeSO_4$, or 150 μM H_2O_2 (positive control). (D) DNase I was used as a positive procedural control. Superscript boxes are close-up of boxed areas. (E–H) Phase contrast images of the same fields shown in A–D. Multilayering cuboidal cells are distinguishable from surrounding fibroblastic cell layer. (I,J) Bright field images of negative controls (cells incubated without terminal deoxynucleotidyl transferase labeling enzyme). (A–J) Original magnification: ×100. Scale bar: 500 μm. Representative results from 1 study. Similar results were observed in 2 independent experiments.

The lowest dose of iron (1 μM), which did not result in increased cellular iron content, also did not produce deleterious effects on osteoblast function or phenotype. This supports Morais et al. [33] who found that a low, 1.5-fold increase in iron during the first week of differentiation only slightly decreased ALP activity and did not affect mineralization.

Table 2
Staining intensity of TUNEL-labeled cells.

Treatment	TUNEL labeling
0	+
5	++
10	++
H_2O_2	+
DNAse I	+++
Neg ctrl	–

Results from 2 independent studies, $n = 1$ to 2 wells per treatment.

In contrast, saturable iron levels appear to have been achieved in the present study at 5 μM and were associated with decreased osteoblast development. At saturable levels, oxidative stress is generally considered the mediator of iron's cytotoxic effects since free iron catalyzes free radical formation through Fenton chemistry [1]. Cytotoxicity due to the oxidative stress brought about by high iron concentrations is supported in the present study by apoptotic cells in the 5 μM and 10 μM treated wells compared to controls. Moderate levels of stained apoptotic cells were observed primarily within and surrounding multilayered nodules, suggesting that cell death among the osteoprogenitor population may contribute to the phenotypic suppression observed during iron overload. However, since cell death did not completely diminish the presence of nodules by the end of the 2-week differentiation period (D20), it is unlikely that apoptosis is the only factor contributing to suppressed phenotype.

The findings from this study suggest that iron affects osteoblast phenotypic development and function after acute exposure as well as during early (D6-15) and late (D15-21) phases of chronic exposure to $FeSO_4$. Introduction of iron to cultures at the beginning of differentiation (D6) resulted in dramatic intracellular alterations of TrfR gene expression between 3 and 24 h after introduction to the media, which was followed by suppressed phenotype markers by D15. This suggests that excess iron may effectively prevent recruitment of non-differentiated cells by interfering with transcription pathways that commit cells to the osteoblast lineage or by contributing to apoptosis of committed osteoprogenitor cells. Researchers have shown that crucial transcription pathways for osteoblast development, including Runx2, Wnt-β catenin, and ERK, are modulated by oxidative stress [34–36].

The presence of multilayered cuboidal cells suggests that iron fails to completely disrupt early stages of osteoblast development but may inhibit matrix maturation and mineralization that occur later in culture.

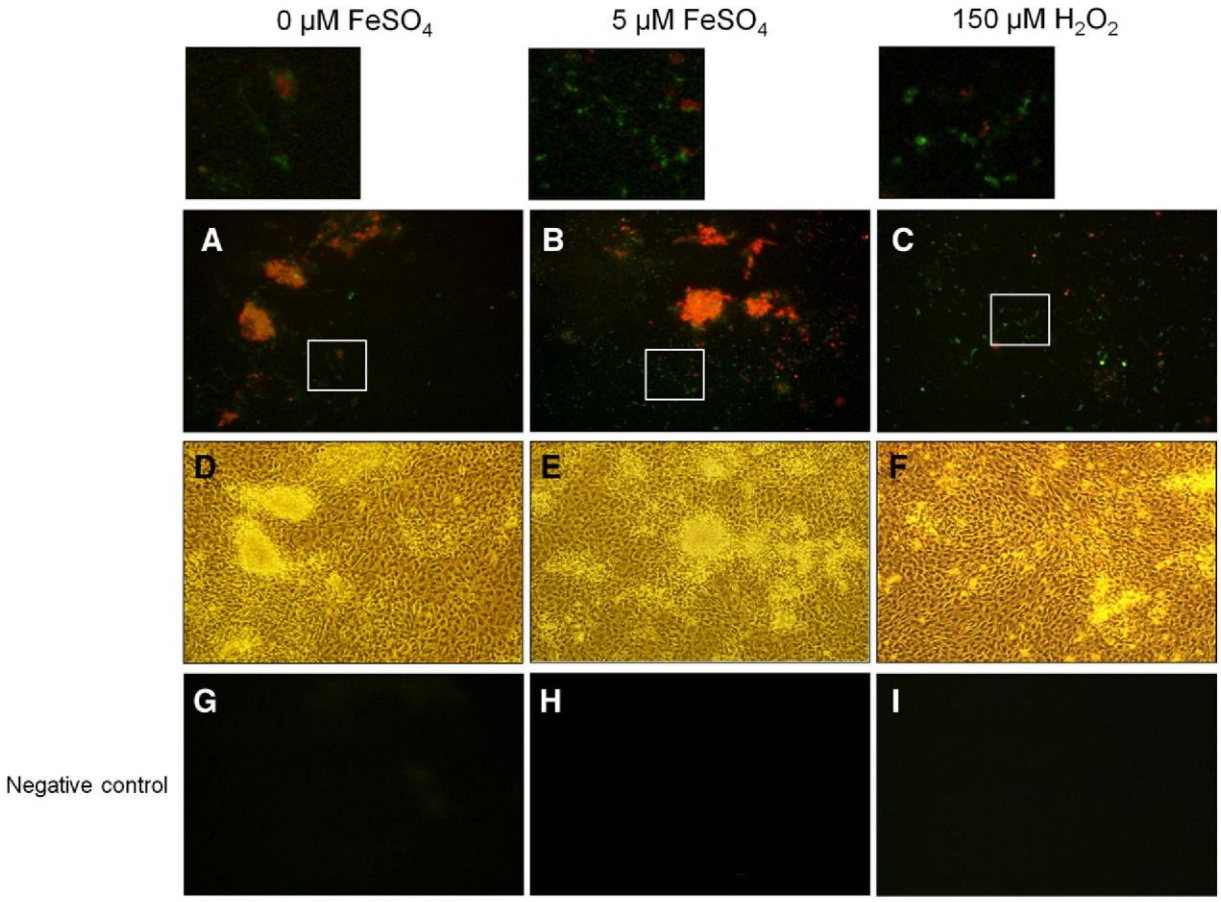

Fig. 7. Annexin V/propidium iodide staining after acute $FeSO_4$ treatment. (A–C) Overlaid green and red fluorescent images of cells treated with 0 or 5 μM $FeSO_4$ for 24 h or 150 μM H_2O_2 (positive control) for 8 h. Superscript boxes are close-up of boxed areas. (D–F) Phase contrast images of the same fields shown in A–C. (G–I) Negative controls (cells incubated in buffer without stain). Similar results were observed in 2 independent experiments.

Moreover, iron overload may elicit additive effects during the later stages of differentiation, as it is well established that osteoblast differentiation and matrix maturation are functionally coupled [37]. Iron has been shown to alter collagen turnover, fibronectin degradation, matrix metalloprotease activity, and expression of cellular adhesion molecules [38–40], all of which are required to form a functional matrix, while proteins, such as OCN and BSP, are thought to be required for mineralization. The additive effects of excessive iron concentrations may also extend to iron pools not associated with the cell layer. This may explain the surprising maximal suppression of osteoblastogenesis and mineralization by the 10 μM dose rather than the 5 μM dose, which had resulted in iron saturation in the cell layer and maximum alteration of iron metabolic proteins. Thus, at the higher dose a free iron pool may exert effects that result in altered osteoblast outcomes independently of iron directly associated with the cell layer. Recently, direct inhibition of hydroxyapatite accumulation by iron in a cell free model has been reported [41].

Table 3
Staining intensity in cells labeled with Annexin V and propidium iodide.

Treatment	Annexin V	Annexin V/propidium iodide
0	+	++
5	++	++
10	++	++
H_2O_2	++	+
Neg ctrl	−	−

Results from 2 independent studies, $n = 1$ to 2 wells per treatment.

In conclusion, intracellular iron accumulation suppresses osteoblast phenotype and function in vitro. Therefore, bone metabolic diseases resulting from iron overload disorders may be attributed to lower numbers of osteoprogenitors due to cell death or decreased recruitment of cells into the osteoblast lineage, a decreased function of cells already committed to the osteoblast lineage, or both. Understanding the exact mechanisms by which iron exerts its effects on osteoblasts will elucidate potential therapies designed to prevent or offset the consequences of low bone mass that arise from iron overload.

References

[1] Crichton RR, Wilmet S, Legssyer R, Ward R. Molecular and cellular mechanisms of iron homeostasis and toxicity in mammalian cells. J Inorg Biochem 2002;91:9-18.
[2] Liu G, Men P, Kenner GH, Miller SC. Age-associated iron accumulation in bone: implications for postmenopausal osteoporosis and a new target for prevention and treatment by chelation. BioMetals 2006;19:245-51.
[3] Appel MJ, Kuper CF, Woutersen RA. Disposition, accumulation and toxicity of iron fed as iron (II) sulfate or as sodium iron EDTA in rats. Food Chem Toxicol 2001;39: 261–9.
[4] Sheth S, Brittenham GM. Genetic disorders affecting proteins of iron metabolism: clinical implications. Annu Rev Med 2000;51:443–64.
[5] Wood JC. Diagnosis and management of transfusion iron overload: the role of imaging. Am J Hematol 2007;82:1132–5.
[6] Guggenbuhl P, Deugnier Y, Boisdet JF, Rolland Y, Perdriger A, Pawlotsky Y, et al. Bone mineral density in men with genetic hemochromatosis and HFE gene mutation. Osteoporos Int 2005;16(12):1809–14.
[7] Mahachoklertwattana P, Sirikulchayanonta V, Chuansumrit A, Karnsombat P, Choubtum L, Sriphrapradang A, et al. Bone histomorphometry in children and adolescents with β-thalassemia disease: iron-associated focal osteomalacia. J Clin Endocrinol Metab 2003;88(8):3966–72.
[8] de Vernejoul MC, Pointillart A, Golenzer CC, Morieux C, BielakoffJ, Modrowski D, etal. Effects of iron overload on bone remodeling in pigs. Am J Pathol 1984;116(3): 377–84.
[9] Matsushima S, Hoshimoto M, Torii M, Ozaki K, Narama I. Iron lactate-induced osteopenia in male Sprague–Dawley rats. Toxicol Pathol 2001;29:623–9.

[10] Matsushima S, Torii M, Ozaki K, Narama I. Iron lactate-induced osteomalacia in association with osteoblast dynamics. Toxicol Pathol 2003;31:646–54.
[11] Kasai K, Hori MT, Goodman WG. Characterization of the transferrin receptor in UMR-106-01 osteoblast-like cells. Endocrinology 1990;126(3):1742–9.
[12] Spanner M, Weber K, Lanske B, Ihbe A, Siggelkow H, Schutze H, et al. The iron-binding protein ferritin is expressed in cells of the osteoblastic lineage in vitro and in vivo. Bone 1995; 17(2):161–5.
[13] Jacobs A, Miller F, Worwood M, Beamish MR, Wardrop CA. Ferritin in the serum of normal subjects and patients with iron deficiency and iron overload. BMJ 1972;4: 206–8.
[14] Eisenstein RS. Iron regulatory proteins and the molecular control of mammalian iron metabolism. Annu Rev Nutr 2000;20:627–62.
[15] Whittaker P, Hines FA, Robl MG, Dunkel VC. Histopathological evaluation of liver, pancreas, spleen, and heart from iron-overloaded Sprague–Dawley rats. Toxicol Pathol 1996;24(5):55–63.
[16] Cooksey RC, Jouihan HA, Ajioka RS, Hazel MW, Jones DL, Kushner JP, McClain DA. Oxidative stress, β-cell apoptosis, and decreased insulin secretory capacity in mouse models of hemochromatosis. Endocrinology 2004;145(11):5305–12.
[17] Carlini RG, Alonzo E, Bellorin-Font E, Weisinger JR. Apoptotic stress pathway activation mediated by iron on endothelial cells in vitro. Nephrol Dial Transplant 2006;21:3055–61.
[18] Bellows CG, Aubin JE, Heersche JNM, Antosz ME. Mineralized bone nodules formed in vitro from enzymatically released rat calvaria cell populations. Calcif Tissue Int 1986;38:143–54.
[19] Davis RJ, Czech MP. Regulation of transferrin receptor expression at the cell surface by insulin-like growth factors, epidermal growth factor and platelet-derived growth factor. EMBO 1986;5(4):653–8.
[20] Erikson KM, Aschner M. Increased manganese uptake by primary astrocyte cultures with altered iron status is mediated primarily by divalent metal transporter. Neurotoxicology 2006;27:125–30.
[21] Bonnelye E, Merdad L, Kung V, Aubin JE. The orphan nuclear estrogen receptor-related receptor α (ERRα) is expressed throughout osteoblast differentiation and regulated bone formation in vitro. J Cell Biol 2001;153(5):971–83.
[22] Liu Y, Parkes JG, Templeton DM. Differential accumulation of non-transferrin-bound iron by cardiac myocytes and fibroblasts.J Mol Cell Cardiol 2003;35:505–14.
[23] Bonnelye E, Chabadel A, Saltel F, Jurdic P. Dual effect of strontium ranelate: stimulation of osteoblast differentiation and inhibition of osteoclast formation and resorption in vitro. Bone 2008;42(1):129–38.
[24] Park BG, Yoo CI, Kim HT, Kwon CH, Kim YK. Role of mitogen-activated protein kinases in hydrogen peroxide-induced cell death in osteoblastic cells. Toxicol 2005;215:115–25.
[25] Aubin JE. Advances in the osteoblast lineage. Biochem Cell Biol 1998;76(6): 899–910.
[26] Cable EE, Connor JR, Isom HC. Accumulation of iron by primary rat hepatocytes in long-term culture: changes in nuclear shape mediated by non-transferrin-bound forms of iron. Am J Pathol 1998; 152(3):781–92.
[27] Popovic Z, Templeton DM. Iron accumulation and iron-regulatory protein activity in human hepatoma (HepG2) cells. Mol Cell Biochem 2004;265:37–45.
[28] Hoepken HH, Korten T, Robinson SR, Dringen R. Iron accumulation, iron-mediated toxicity and altered levels of ferritin and transferrin receptor in cultured astrocytes during incubation with ferric ammonium citrate. J Neurochem 2004;88:1194–202.
[29] Beauchamp JR, Woodman PG. Regulation of transferrin receptor recycling by protein phosphorylation. Biochem J 1994;303(Pt 2):647–55.
[30] van Driel IR, Goding JW. Heterogeneous glycosylation of murine transferrin receptor subunits. Eur J Biochem 1985; 149:543–8.
[31] Torti FM, Torti SV. Regulation of ferritin genes and protein. Blood 2002;99(10): 3505–16.
[32] Toth I, Bridges KR. Ascorbic acid enhances ferritin mRNA translation by an IRP/ aconitase switch. J Biol Chem 1995;270(33):19540–4.
[33] Morais S, Dias N, Sousa JP, Fernandes MH, Carvalho GS. In vitro osteoblastic differentiation of human bone marrow cells in the presence of metal ions. J Biomed Mater Res 1999;44:176–90.
[34] Hinoi E, Fujimori S, Wang L, Hojo H, Uno K, Yoneda Y. Nrf2 negatively regulates osteoblast differentiation via interfering with Runx2-dependent transcriptional activation. J Biol Chem 2006;281(26):18015–24.

[35] Bai X, Lu D, Bai J, Zheng H, Ke Z, Li X, Luo S. Oxidative stress inhibits osteoblastic differentiation of bone cells by ERK and NF-κB. Biochem Biophys Res Comm 2004;314:197–207.
[36] Almeida M, Han L, Martin-Millan M, O'Brien CA, Manolagas SC. Oxidative stress antagonizes Wnt signaling in osteoblast precursors by diverting β-catenin from T-cell factor- to Forkhead box O-mediated transcription. J Biol Chem 2007;282(37): 27298–305.
[37] Owen TA, Aronow M, Shalhoub V, Barone LM, Wilming L, Tassinari MS, Kennedy MB, Pockwinse S, Lian JB, Stein GS. Progressive development of the rat osteoblast phenotype in vitro: reciprocal relationships in expression of genes associated with osteoblast proliferation and differentiation during formation of the bone extracellular matrix. J Cell Physiol 1990:420–30.
[38] Gardi C, Arezzini B, Fortino V, Comporti M. Effect of free iron on collagen synthesis, cell proliferation and MMP-2 expression in rat hepatic stellate cells. Biochem Pharmacol 2002;64:1139–45.
[39] Bilello JP, Cable EE, Isom HC. Expression of E-cadherin and other paracellular junction genes is decreased in iron-loaded hepatocytes. Am J Pathol 2003; 162 (4): 1323–38.
[40] Zardeneta G, Milam SB, Schimtz JP. Iron-dependent generation of free radicals: plausible mechanisms in the progressive deterioration of the temporomandibular joint. J Oral Maxillofac Surg 2000;58:302–8.
[41] Guggenbuhl P, Filmon R, Mabilleau G, Baslé MF, Chappard D. Iron inhibits hydroxyapatite crystal growth in vitro. Metabolism 2008;57:903–10.